

Polymerizable Ionic Liquid-derived Non-precious Metal Catalyst Fe-N/C for Oxygen Reduction Reaction

Guogang Xue^{1,*}, Jianjun Tian², Jun Bao³, Dan Hu³

¹ School of Physics and Electronic Engineering, Kewen College, Jiangsu Normal University, Xuzhou 221116, P.R. China

² School of Environmental and Chemical Engineering, Tianjin Polytechnic University, Tianjin 300387, P.R. China

³ Wuxi Test Institute of Supervision & Inspection on Product Quality, Wuxi 214101, P.R. China

*E-mail: ggxue@jsnu.edu.cn

Received: 10 October 2020 / Accepted: 15 November 2020 / Published: 30 November 2020

Polymerizable ionic liquid (PIL) of hydrolyzed vinyl imidazolium nitrate ([HVim]NO₃) was used to prepare the non-precious metal catalyst (NPMC) of Fe-N/C. The material was characterized for catalytic performance toward oxygen reduction reaction (ORR). The onset and half wave potential for ORR is 0.90 and 0.64 V_{RHE}, respectively. The electrochemical tests show that the Fe-N/C material is a potential NPMC for ORR. Therefore, the PIL is a promising precursor for ORR catalyst free of noble metal.

Keywords: Polymerizable ionic liquid; Non-precious metal catalyst; Oxygen reduction reaction; Fuel cell

1. INTRODUCTION

Oxygen reduction reaction (ORR) is highly important for green and renewable power sources such as metal-air batteries and fuel cells [1-5]. Unfortunately, the ORR is sluggish, and electrocatalysts are required [6]. Until now, the optimal electrocatalysts for ORR are still Pt-based catalysts. However, the high cost of the precious metals such as Pt and Ir became a primary barrier to the mass application of metal-air batteries and fuel cells [7]. Therefore, finding low-price and efficient non-precious metal catalyst (NPMC) for ORR has been considered an important aim for decades [8]. The carbon supported materials (M-N/C, M= Co, Fe, Ni, Mn, etc.) prepared by the pyrolysis of a series of precursor materials containing metal, nitrogen and carbon are considered as promising catalysts [9, 10]. Excellent reviews can be found in several literatures [6, 9, 11].

The precursor providing N and C is important for M-N/C because it affects the simplicity of the

preparing process and the catalytic performance [12]. Recently, ionic liquids (ILs) are attracting considerable interest as precursors for M-N/C [13, 14]. ILs are salts with low melting points [15, 16]. The ILs possess several unique properties such as negligible vapor pressure, functional designability, and high C, N content. These properties render the ILs as a kind of promising precursor for M-N/C. Polymerizable ionic liquids (PILs) is an important group of ILs, and have been interested as novel precursors for NPMCs [17]. PILs combines the advantages of both polymers and ILs [18]. During the pyrolysis process, the carbon networks of polymer may produce various carbon material [19]. Additionally, the heteroatoms in the PILs remain incorporated within the carbonaceous scaffolds, creating heteroatom doped carbon [20]. Simultaneously, the polymers' shortage of generating low-molecular-weight organic compounds because of heat decomposition is avoided [21]. Our research group reported the preparation of the Co-N/C catalyst with PIL of vinyl imidazolium dihydrogen phosphate ([Hvim]H₂PO₄), and considerable ORR catalytic performance was obtained [17]. Later, the work was improved by replacing the H₂PO₄⁻ with NO₃⁻, which can "explode" during the pyrolyzing process to fabricate the carbon nanosheets [22]. However, the high price of Co remains a potential problem for the future application [23-25]. Although metal-free NPMC has been prepared with [Hvim]NO₃ [26], the metal-free catalyst is still on a less competitive level comparing with the NPMCs containing metal [27, 28]. Therefore, preparing the NPMC containing metal is of high interest. Besides the Co-N/C and metal-free NPMCs, the Fe-N/C is an important analog. Thus, it is highly interesting to investigate the preparation of Fe-N/C material with PIL as the precursor. However, this investigation has not been conducted although [Hvim]NO₃ can be a promising precursor for Fe-N/C considering its unique property.

Herein, by continuing our previous work, the Fe-N/C was prepared using the PIL of [Hvim]NO₃ as the precursor. The prepared Fe-N/C shows a promising catalytic performance for ORR. The results demonstrate the great potential of PIL as the precursor for electrocatalyst free of noble metal.

2. EXPERIMENTAL

2.1 Synthesis of polymerizable ionic liquid

The [Hvim]NO₃ was prepared with the process described in the previous work [22]. Briefly: an equal mol of HNO₃ (65% wt) was added dropwise to N-vinyl imidazolium (95% wt) while stirred at room temperature. The system was further stirred for an hour after the adding process. Then the system was transferred to a water bath of 50 °C and stirred for 2 h to obtain a viscous liquid, i.e. PIL of [Hvim]NO₃.

2.2 Preparation of the Fe-PIL catalyst by heat-treatment

To investigate the factors influencing the catalytic performance, the catalysts were prepared under various conditions. Take the following as an example: 0.1 mol of the PIL obtained above and a

0.1/3 mol of $\text{Fe}(\text{NO}_3)_3 \cdot 9\text{H}_2\text{O}$ was dissolved in 50 mL of ethanol, separately. The system was stirred for about 2 h. Subsequently, the $\text{Fe}(\text{NO}_3)_3$ solution was added dropwise to the PIL solution while keeping the system stirred. Fine sediments appeared immediately. The system was continuously stirred for 6 h. The sediments were collected after the ethanol was removed by filtering and then dried at 60 °C for an hour.

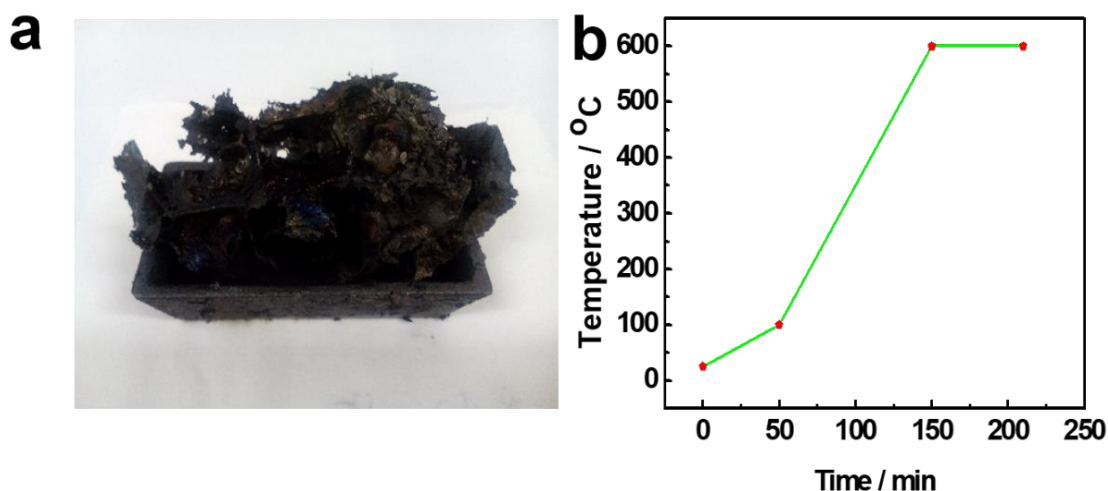


Figure 1. (a) As-prepared catalyst sample, (b) the heating process temperature-time curve.

2.5 g of the solid obtained above was pyrolyzed in a furnace under the N_2 atmosphere at 600 °C for an hour to get a black sample as shown in Figure 1a. The temperature-time curve is presented in Figure 1b. During the heat-treatment process, the $[\text{Hvim}]\text{NO}_3$ shall polymerize as shown in the previous works [22, 26]. At around 170 °C, an “explode” shall take place with yellow smoke. However, the experiment is safe since only 2.5g of the solid is used. The whole preparing process is presented in Figure 2.

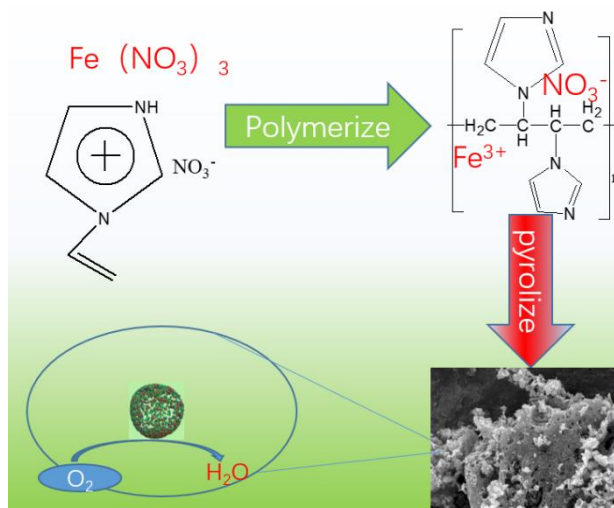


Figure 2. Schematic illustration of the catalyst preparation process.

To investigate the temperature influence, the Fe-N/C was prepared at 600, 700 and 800 °C, and

the corresponding samples are defined as Fe₃-600, Fe₃-700, and Fe₃-800, respectively.

The influence of Fe content was investigated by preparing the catalyst with various ratio of Fe(NO₃)₃ to [Hvim]NO₃. For 0.1 mol of the PIL, 0, 0.01, 0.033 and 0.04 mol of Fe(NO₃)₃·9H₂O was added. The samples were prepared at 600 °C, and are denoted as Fe₀-600, Fe₁-600, Fe₃-600, and Fe₄-600, respectively. The resulted samples were characterized for catalytic performance toward ORR.

2.3 Physical characterization of electrocatalyst

The morphology of the synthesized samples was investigated by scanning electron microscopy (SEM) on JEOL JSM-7100F. The surface compositions of the synthesized electrocatalysts were analyzed by X-ray photoelectron spectroscopy (XPS) on PHI Quantera ii and SEM-EDX on JEOL JSM-7100F. The X-ray diffraction (XRD) measurement was performed on D8 Discover (Bruker). The specific surface area of the samples was measured via nitrogen adsorption on a Micromeritics ASAP 2020.

The Raman spectra were obtained at room temperature on a Horiba Xplora Plus spectrometer equipped with an optical multichannel analyzer with 532 nm laser excitation. The spectra were recorded between 100 and 4000 cm⁻¹ through a 50× objective lens.

2.4 Electrochemical measurements

Electrochemical measurements were conducted on a CHI760E electrochemical workstation with a three-electrode system. An Hg/HgO and Pt wire were used as the reference and counter electrode, respectively. A glassy carbon electrode (GCE, 5 mm in diameter) carrying the sample was used as the working electrode, which was prepared as described elsewhere. Briefly: 2.5 mg of the prepared catalyst powder with 450 μL ethanol and 50 μL Nafion solution (5wt% from Aldrich) was sonicated for 30 minutes to form a uniform ink. 10 μL of the ink was dropped on the surface of the pre-treated GCE, yielding a loading of 0.25 mg cm⁻². The electrode was dried in ambient temperature for an hour before use.

Cyclic voltammetry (CV) and linear sweep voltammetry (LSV) were recorded in N₂- or O₂-saturated 0.1 M KOH solution in water. Electrode potential was converted relative to the reversible hydrogen electrode (RHE) potential from the Hg/HgO electrode using: $E_{(RHE)} = E_{(Hg/HgO)} + 0.93$ V.

The stability test for ORR was performed for 3600 s at 0.73 V_{RHE} in O₂-saturated 0.1 M KOH solution.

3. RESULTS AND DISCUSSION

3.1 Electrochemical characterizations

The catalytic performance was investigated with CV technology, and the CV curves for Fe₃-600 in N₂- and O₂-saturated electrolyte are shown in Figure 3a. No significant response was observed

when the electrolyte was saturated with nitrogen. However, when the electrolyte was saturated with oxygen, an obvious current increase appeared, implying an electrocatalytic activity of the Fe₃-600 for ORR.

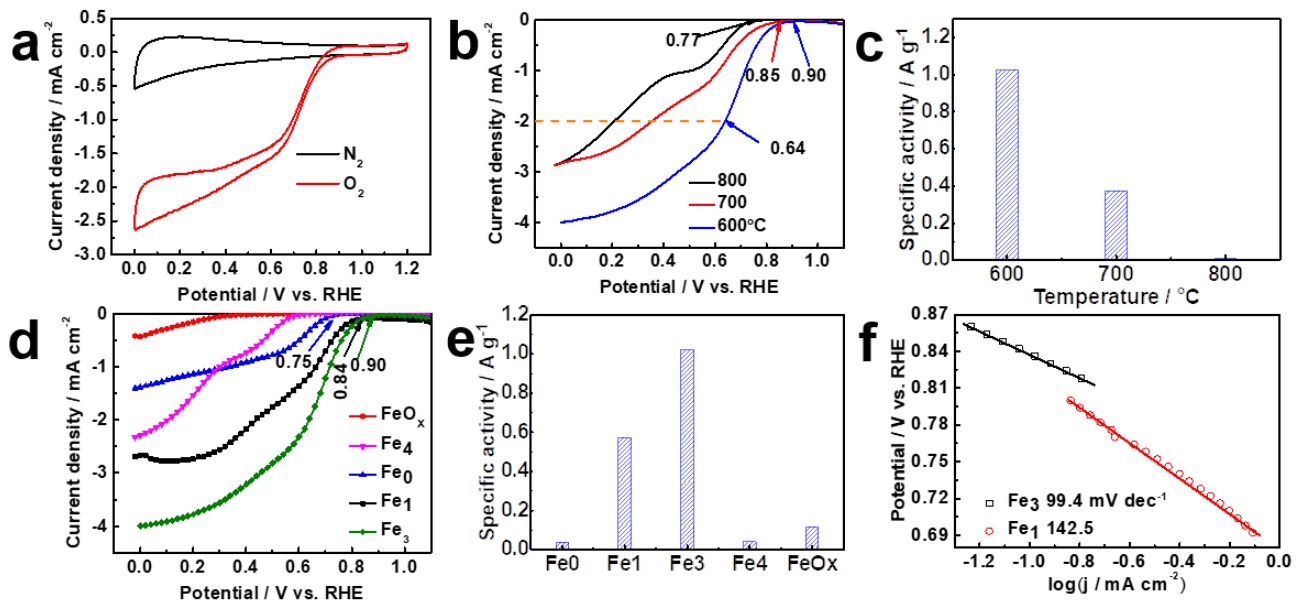


Figure 3. (a) CV curves for Fe₃-600 in N₂- and O₂-saturated electrolyte, (b) LSV curves for ORR of Fe₃-600, 700 and 800, (c) specific activity for ORR with various temperature, the current at 0.80 V_{RHE}, (d) LSV curves for ORR of sample with various Fe content, (e) specific activity for ORR with various Fe content at 0.80 V_{RHE}, (f) Tafel plots for Fe₃ and Fe₁.

To investigate the effect from temperature on the catalytic performance, the Fe-N/C prepared at various temperatures was characterized, and the LSV curves for ORR are presented in Figure 3b. The sample prepared at 600 °C demonstrates the highest catalytic performance, and the performance decreases with increase in pyrolyzing temperature. The onset potential of Fe₃-600 is 0.90 V_{RHE}, higher than that of Fe₃-700 and Fe₃-800, which are 0.85 and 0.77 V_{RHE}, respectively. Additionally, the half wave potential for Fe₃-600 is 0.64 V_{RHE}. This is comparable with values reported by some of literatures as shown in Table 1. The results show the obvious temperature influence on the catalytic performance. The influence from temperature on the catalytic performance of the Fe-N/C was also reported by other work [29].

Table 1. Reported catalytic performance.

Catalyst	Precursor/condition	On set Potential/ V _{RHE}	Half wave potential/ V _{RHE}	Specific current /A g ⁻¹ at 0.8 V _{RHE}	Reference	Year
Fe/N/C HNSs-750	Fe ³⁺ -PDA/SiO ₂ /750 °C, Ar, 2 h	0.89	0.72	0.58	[30]	2015
N-doped porous graphene foam	GO (graphene oxide), FeCl ₂ ·4H ₂ O, dicyandiamide, silica spheres/900 °C, N ₂ , 1	1.02	0.86	12.4	[31]	2015

	h					
N, P co-doped carbon	Supermolecular aggregate of self-assembled melamine, phytic acid and graphene oxide (MPSA/GO)/1000 °C, Ar, 1 h	~0.95	~0.81	22.9	[32]	2016
Graphene quantum dots	Graphitized carbon nanofibers/120 °C, reflux, 2 h	~0.84	0.67	1.3	[33]	2016
Co ₃ O ₄	Co(NO ₃) ₂ ·6H ₂ O (0.055g) and glycerol (4.0 mL) dissolved in isopropanol/700 °C, Ar, 200 min	0.93	0.84	13.7	[34]	2016
N-doped carbon	Polyimide film/1000 °C, Ar, 1 h	0.97	0.82	29.4	[35]	2016
N, S co-doped carbon	Pyrrole, aniline, ammonium persulfate heated to various temperatures for 2 h at an increasing rate of under flowing N ₂	0.93	0.81	7.13	[36]	2016
Co-N co-doped hollow carbon sphere	Poly methyl methacrylate, cobalt acetate/800 °C, N ₂ , 5 h	0.96	0.86	16.7	[37]	2017
N-doped GO	GO in ammonia/5 °C, ultrasonic treatment, 5 min	0.84	0.7	0.98	[38]	2017
Co-N/C	Co(NO ₃) ₂ + [Hvim]NO ₃ /600 °C, N ₂ , 1 h	0.96	0.8	7.85	[22]	2017
Mn ₃ O ₄ nanoparticles on layer-structured Ti ₃ C ₂	Ti ₃ C ₂ MXene, Mn(AC) ₂ /150 °C, 3 h	0.89	0.8	25	[39]	2017
N,P co-doped carbon	[Hvim]H ₂ PO ₄ /560 °C, N ₂ , 1 h	0.93	0.75	7.7	[40]	2018
Fe-N-C	Fe(NO ₃) ₃ ·9H ₂ O, nicarbazin, methylimidazole, glucoril, the mixture of urea, zinc, carbon nanotube and LM150 fumed silica/975 °C, N ₂ , 45 min	0.96	0.83	N/A	[41]	2018
N, P dual-doped carbon	Melamine-diphenylphosphinic acid complex crystals/1100 °C, N ₂ , 1 h	0.91	0.79	7.85	[42]	2018
N, S co-doped carbon	Acetylene black, melamine and sulphur template/900 °C, vacuum, 1 h	0.99	0.82	9.44	[43]	2018
Ultrathin nitrogen-doped holey carbon	GO, zinc gluconate/900 °C, Ar, time unavailable	0.97	0.82	17.6	[44]	2018
Fe-N-C	Glycine, citric acid, and FeCl ₃ /800 °C, N ₂ , 2 h	0.93	0.75	8	[45]	2018
Graphdiyne doped with sp-hybridized nitrogen	Few-layer oxidised graphdiyne, melamine/900 °C, Ar, 3 h	~1.0	0.87	9.32	[46]	2018
Pyridinic-N-dominated doped defective graphene	C ₃ N ₄ -GO/900 °C, N ₂ , 3 h	0.98	0.85	27.2	[47]	2018
FeN ₄ moiety/MXene	Ti ₃ C ₂ T _x MXene and a certain amount of pure FePc powder/stirred 20 h	~0.93	0.86	20.8	[48]	2018
Fe-N ₄ embedded carbon fabric	GO, polyacrylonitrile, FeCl ₃ /900 °C, NH ₃ , 1 h	0.93	0.73	N/A	[49]	2019
N-doped carbon	Citric acid and NH ₄ Cl/1000 °C, Ar, 3 h	0.95	0.82	19.62	[50]	2019
N-doped porous carbon	D-gluconic acid sodium salt/700 °C, Ar, 1 h	0.94	0.864	19	[51]	2019
Nitrogen-doped porous carbon	Bio-MOF-1 Zn ₈ (Ad) ₄ (Bpdc) ₆ O·2Me ₂ NH ₂ ·8DMF·11H ₂ O /1000 °C, Ar, 1,2,3,4 h	0.96	0.84	9	[52]	2019
S, N, F triple-doped porous carbon	Superfine PTFE, thiourea/ 1000 °C, Ar, 1 h	0.98	0.86	11.77	[53]	2019
Epichlorohydrin-dimethylamine copolymer modified CNT	Epichlorohydrin-dimethylamine copolymer modified CNT/70 °C, 24 h	0.87	0.7	0.2	[54]	2019
Fe-N/C	Fe(NO ₃) ₃ ·9H ₂ O+[Hvim]NO ₃ /600 °C, N ₂ , 1 h	0.9	0.64	1.02	This work	2020

Figure 3c shows the specific activity per mass of the samples prepared at different temperatures at 0.80 V_{RHE}. The specific activity of Fe₃-600 is the highest among the tested samples and a value of 1.02 A g⁻¹ (18.58 mA m⁻²) was obtained. Some literature values for the specific activity per real surface area are 7.5 mA m⁻² [4], 3.9 mA m⁻² [55] and 27.3 mA m⁻² [56]. So, the specific activity of the sample in the present work is comparable to these reported values.

The Fe-content influence on the catalytic performance for ORR was studied. Figure 3d shows the LSV curves for ORR of Fe₀-600, Fe₁-600, Fe₃-600 and Fe₄-600. The catalytic performance for

ORR is rather poor when no iron was introduced, and an onset potential of around 0.75 V_{RHE} was observed for Fe₀-600. The performance was improved when iron was introduced, and the ORR onset potential of 0.84 and 0.90 V_{RHE} was observed for Fe₁-600 and Fe₃-600, respectively. However, when 0.04 mol Fe(NO₃)₃ was added to 0.1 mol PIL, namely the Fe₄-600, the catalytic performance decreased drastically lower than that of Fe₀-600. The results show that a reasonable Fe content is important for the preparation of Fe-N/C derived from PIL. The specific activities per mass of the samples with various Fe content are presented in Figure 3e. The Fe-N/C possesses activity higher than that of FeO_x (without carbon) and Fe₀ (N-doped carbon without Fe). Moreover, the Tafel slope of Fe₁ is much higher than that of Fe₃ as shown in Figure 3f. Therefore, the higher specific activity, the higher onset potential and the lower Tafel slope make Fe₃ the optimist catalyst for ORR among the samples.

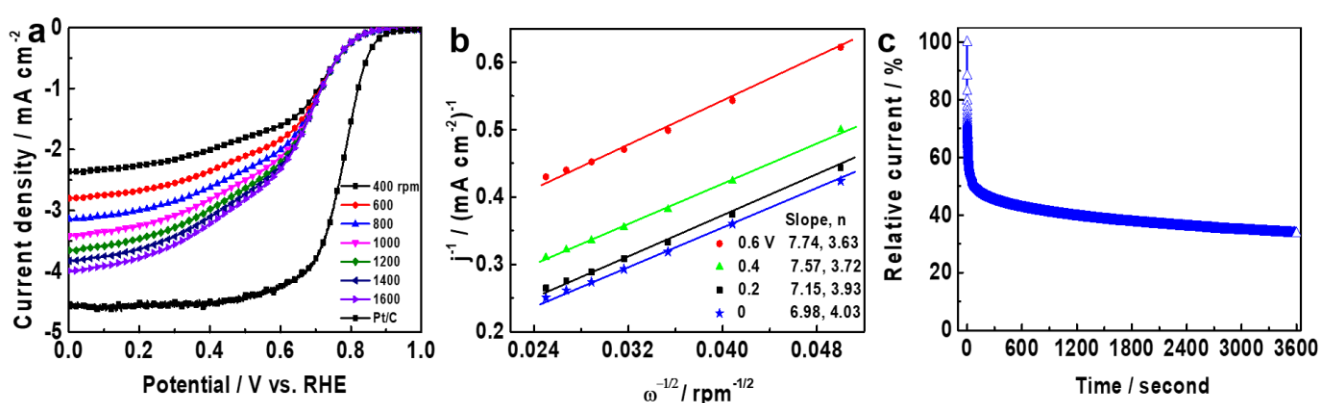


Figure 4. (a) LSV curves for ORR of Fe₃-600 at various rotational rates and the LSV of commercial Pt/C (20% wt) at 1600 rpm, (b) K-L plots of Fe₃-600, (c) stability for ORR of Fe₃-600.

Subsequently, the Fe₃-600 with the best catalytic performance was further investigated with rotating disk electrode (RDE) technology for the ORR catalytic performance. The LSV curves at various rotational rates presented in Figure 4a confirm the electrocatalytic performance of Fe₃-600. An onset potential of 0.90 V_{RHE} is observed, nearing that of other reported materials [4]. The LSVs demonstrate a typical current increase with higher rotational speed. This is caused by the thinner diffusion layer at higher rotating rates. Subsequently, the number of apparent electrons transferred (n) was investigated. A group of lines called K-L plots shown in Figure 4b were constructed according to Figure 4a by plotting j^{-1} versus $\omega^{-1/2}$ at various potentials. The K-L plots demonstrate a linearity at each potential, indicating a first-order reaction kinetics with respect to the concentration of dissolved O₂.

The n was calculated via eq. (1) and (2), where j and j_k are the measured and kinetic current densities, respectively. B is the reciprocal of slope of K-L plots, F is the Faraday constant (96485 C mol⁻¹), C_0 is the bulk concentration of O₂ (1.2×10^{-3} mol L⁻³), D_0 is the diffusion coefficient of O₂ in 0.1 M KOH (1.9×10^{-5} cm² s⁻¹) and γ is the kinetic viscosity of the electrolyte (0.01 cm² s⁻¹). The constant 0.2 is adopted when the rotation speed (ω) is expressed in rpm [57]. The calculated n is 3.63~4.03. This value is comparable with that of the 4e-pathway of other N doped carbon materials,

raging in 3.2~4.1 [27, 28]. The n implies that the ORR of the sample is via a four-electron pathway, which is favorable for power sources.

$$1/j = 1/j_k + 1/B\omega^{0.5} \quad (1)$$

$$B = 0.2nFC_0D_0^{2/3}\gamma^{-1/6} \quad (2)$$

The stability for ORR of Fe₃-600 was tested, and the result is presented in Figure 4c. The ORR can maintain about 40%. Of course, the catalytic performance is still lower than that of the commercial Pt/C. However, the lower performance can be justified by the much lower price of the prepared sample.

3.2 Physical characterizations

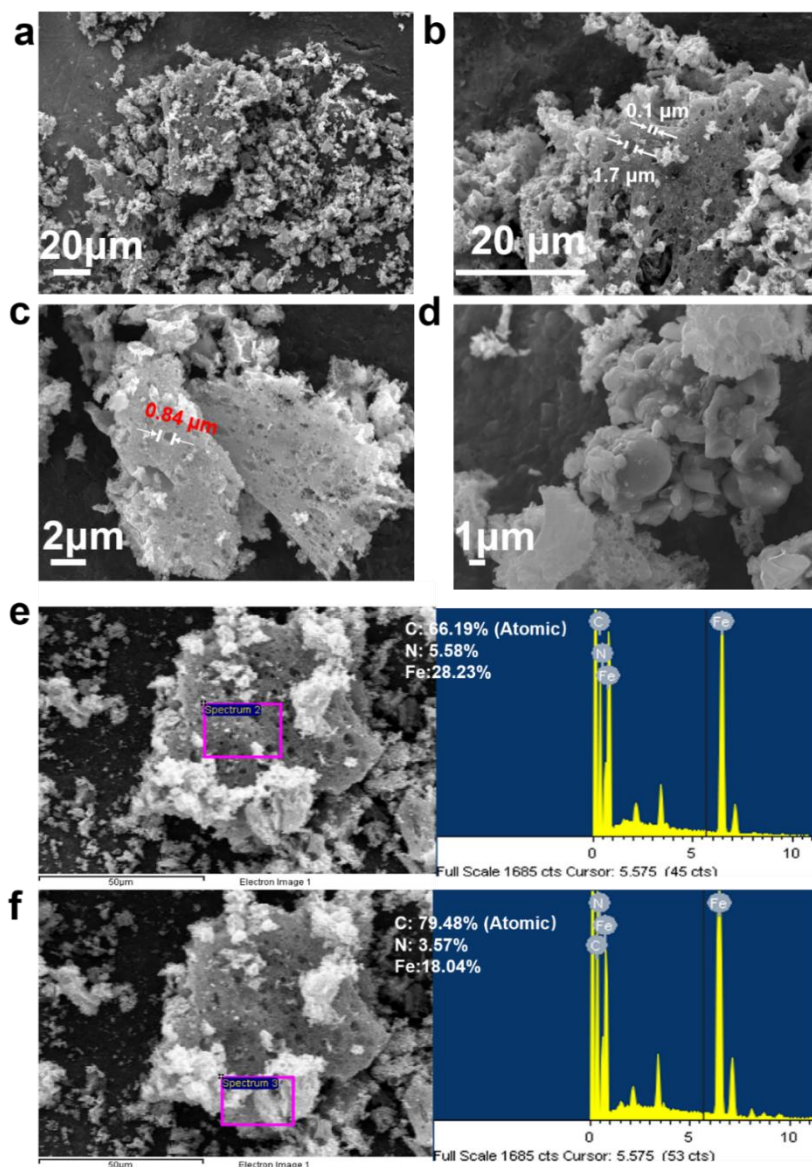


Figure 5. SEM images of Fe₃-600, (a) preliminary image of the sample, (b) image at higher magnification, (c) image of the white solids, (d) image of Fe₃-800, (e) EDX spectra of Fe₃-600 of grey zone and (f) white zone.

Figure 5a shows the SEM image of Fe₃-600. Scattered irregular solids can be observed. Figure 5b is the image of Figure 5a at higher magnification. Porous structure is demonstrated, and pores sizing from hundreds of nanometers to several microns is shown. The small white solids were investigated at higher magnification, and the image is presented in Figure 5c. It demonstrates that the white solids are also porous, and pores with diameters lower than 1 μm are demonstrated. The pores may be fabricated by the decomposition of the NO₃⁻. The porous structure is favorable to improve the catalytic performance. Figure 5d is the SEM image of Fe₃-800. The porous structure disappears when the sample was prepared at 800 °C. The disappearing of the pores may cause decrease of active sites accessible to the reacting species, resulting in lower catalytic performance. This may be one of the reasons explaining the lower catalytic performance of the sample prepared at higher temperature.

The compositions of the grey and white zones were investigated with SEM-EDX method, and the results are presented in Figure 5e and Figure 5f, respectively. The C content for the white zone increased comparing with that of the grey zone. However, the N and Fe content for the white zone is lower than those of the grey zone. Figure 5 confirms that the carbon doped with Fe and N was successfully prepared.

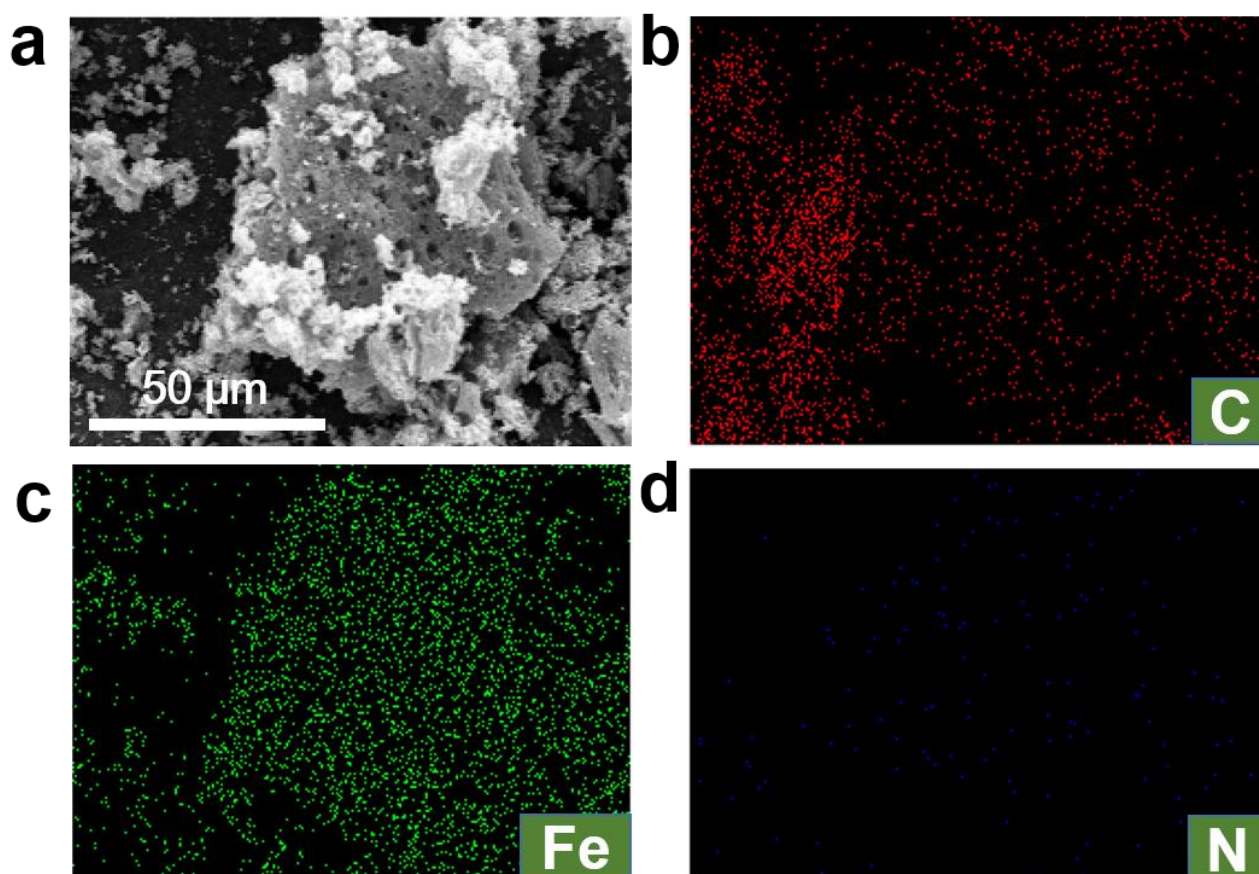


Figure 6. SEM-EDX elemental mapping images of Fe₃-600: (a) SEM image, (b) C, (c) Fe, (d) N.

Furthermore, to investigate the elemental distribution of the prepared sample, the mapping

images of carbon, nitrogen, and iron obtained using SEM-EDX spectroscopy are shown in Figure 6. The mapping images for C, Fe and N are presented in Figure 6b-d, respectively. It is evident that the as-prepared sample contains carbon, nitrogen and iron. The images show that the metal and N were incorporated with carbon uniformly.

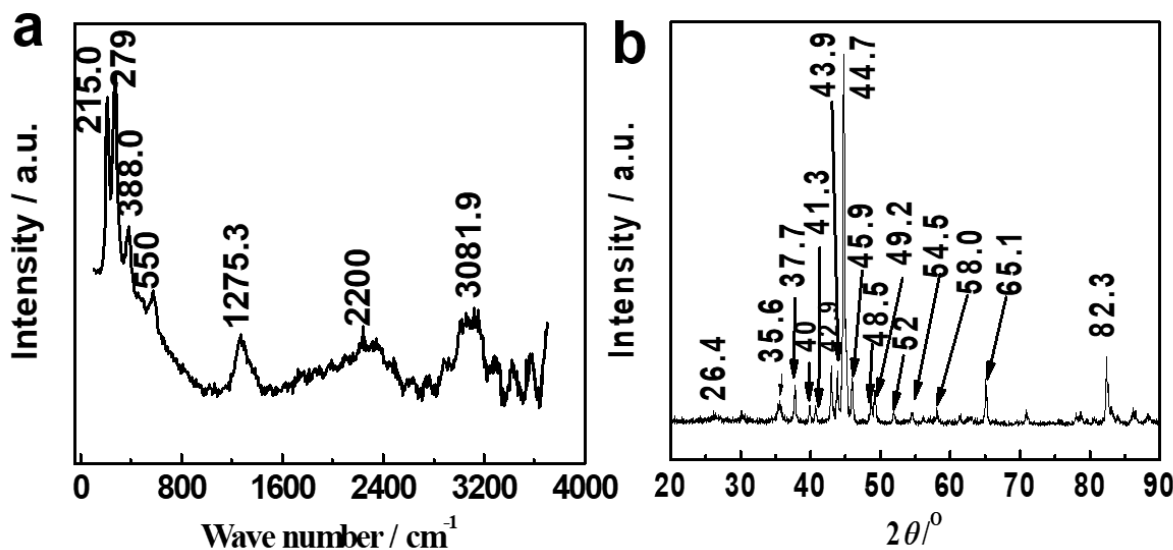


Figure 7. (a) Raman spectra, (b) XRD pattern of Fe₃-600.

The Raman spectra of Fe₃-600 are presented in Figure 7a. The peak at 388 and 550 cm⁻¹ can be assigned to iron oxide [58]. The peaks at 215 and 279 cm⁻¹ are like those of Fe₃O₄ [59]. The peak at 1275.3 cm⁻¹ is generally attributed to the D-band of graphite, and this peak corresponds to the disordered graphite structures [60]. The peak 2200 cm⁻¹ can be assigned to CN stretching [61]. The peak at 3081.9 cm⁻¹ can be assigned to O-H vibration [62]. Therefore, the Raman spectra show that the carbon doped with nitrogen and Fe was obtained.

Further, the Fe₃-600 was investigated for crystallography with XRD method, and the pattern is presented in Figure 7b, and the peaks are demonstrated. The assignments of these peaks are: The peaks at 26.4° and 54.5° are for graphite [63]. 35.6° can be assigned to Fe₂O₃ [64]. The peak at 37.7°, 40°, 45.9°, 48.5°, 49.2° and 58° can be assigned to Fe₃C [64, 65]. The peak at 42.9° is of γ -Fe [64]. The peak at 44.7° can be assigned to Fe BCC(110) [66]. The peak at 65.1° can be assigned to Fe(200) [67]. The peak near 44° suggests the possibility of either amorphous phase or material with a nanocrystalline grain structure [68]. The peak at 52° and 82.3° is of α -Fe [69, 70]. The XRD results also imply the carbon doped with iron was obtained.

The XPS measurements were performed to monitor the doping levels, and the results are presented in Figure 8. Figure 8a shows the XPS survey spectra, the peaks for C 1s (79.6%, atomic), N 1s (4.0%), and O 1s (15.3%) and Fe 2p (1.1%). The results show that the sample is composed of mainly carbon doped with heteroatoms of N and O.

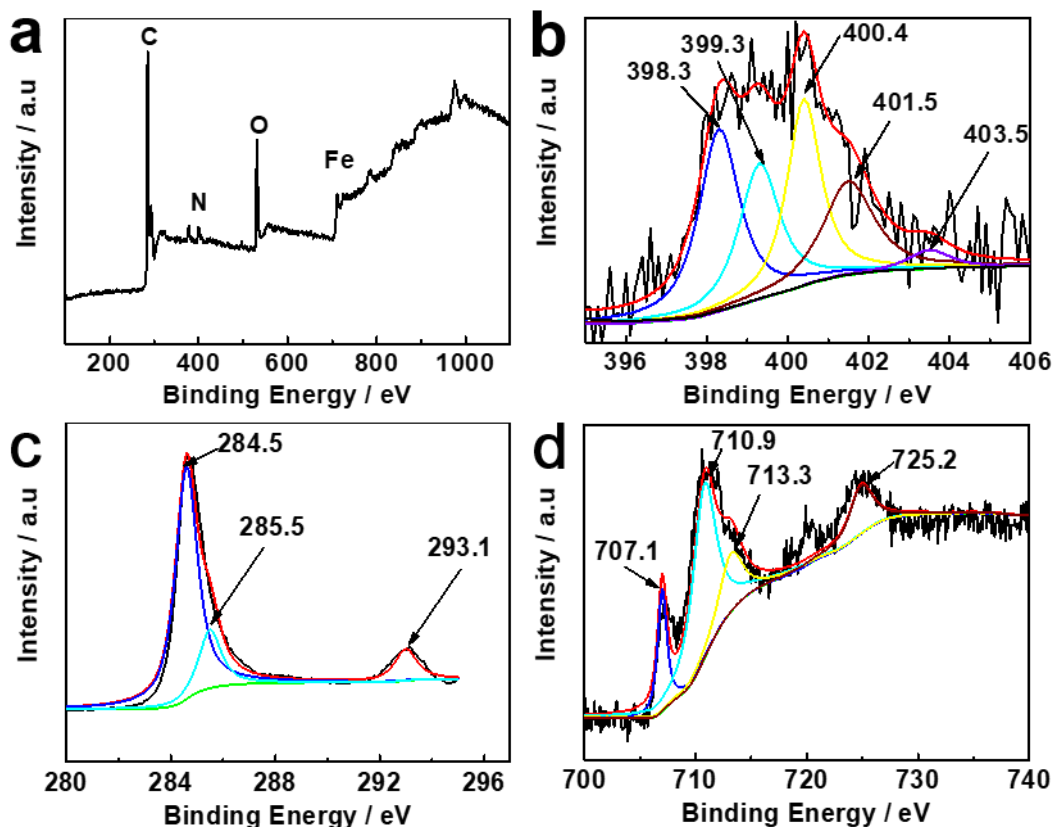


Figure 8. XPS survey spectra of Fe₃-600, (a) survey, (b) N 1s, (c) C 1s, (d) Fe 2p.

High resolution N 1s XPS spectra were deconvoluted into four peaks as shown in Figure 8b. N is present in the forms of pyridinic N (398.3 eV, 27.32%) [71], cyanide N and (or) pyridine N (399.3 eV, 26.43%) [72], pyrrolic N (400.4 eV, 23.52%) [73], graphitic N (401.5 eV, 18.21%) [74], and oxidized N (403.5 eV, 4.52%) [75]. For the stronger electronegativity of N, the charge will be redistributed, which is helpful to enhance the catalytic performance [76, 77]. The pyridinic and graphitic N are helpful to improve the catalytic ability since they are highly active and stable catalytic centers for ORR [78]. The pyridinic nitrogen with a lone electron pair can form side-on adsorption of oxygen molecule to weaken O-O bonding, and the graphitic nitrogen facilitates electron transfer from the carbon electronic bands to the antibonding orbitals of oxygen [79, 80]. Pyrrolic N is also conducive to enhance the ORR catalytic performance [81].

Figure 8c shows the C 1s XPS spectra. The peaks at 284.5 and 285.5 eV can be attributed to the C-C carbon, C-O and/or C-N carbon, respectively [26]. The peak at 293.1 eV is attributed to the sp²-hybridized C atoms in the aromatic ring attached to terminal uncondensed amino groups (e.g. -NH₂ and -NH) [82].

Figure 8d shows the XPS spectra of Fe. The peak at 707.1 eV can be assigned to coordinated Fe atoms [83]. The peak at 710.9 eV is assigned to surface Fe³⁺ species [83], the peak at 713.3 and 725.2 eV can be assigned to Fe 2p_{3/2} and Fe 2p_{1/2}, respectively [84, 85].

The XPS and other physical characteristics show that the PIL can be used as precursor to prepare Fe-N/C. The electrochemical tests show that the prepared sample possesses considerable

catalytic performance for ORR.

The specific surface areas of the samples were measured to calculate the specific activity per real surface area. The Brunauer Emmett Teller (BET) surface areas of the samples are presented in Table 2. For the Fe₃ derived from the PIL, the surface area was found to decrease with increase in the pyrolyzing temperature. This may be one reason for the Fe₃ catalytic performance decrease at elevated pyrolyzing temperature.

Table 2. BET surface areas of the catalysts.

Sample	Fe ₁ -600	Fe ₃ -600	Fe ₄ -600	Fe ₃ -700	Fe ₃ -800
Surface area /m ² g ⁻¹	59.57	54.90	62.25	32.67	23.65

4. CONCLUSIONS

A process to prepare Fe-N/C catalyst free of noble metal with polymerizable ionic liquid was described. The prepared sample was then investigated as catalyst for ORR. Considerable catalytic performance for ORR was observed. The onset potential of 0.90 V_{RHE}, and a half wave potential of 0.64 V_{RHE} in 0.1 M KOH solution for ORR was obtained. The influences from pyrolyzing temperature and Fe content on the catalytic performance for ORR were investigated. All the results imply the promising potential of PIL as precursor for non-precious metal catalyst toward ORR in alkaline electrolyte.

ACKNOWLEDGEMENTS

This work is financially supported by PAPD (A Project Funded by the Priority Academic Program Development of Jiangsu Higher Education Institutions), the Natural Science Research Project of Jiangsu Higher Education Institutions (Grant No. 17KJB480005), the National Natural Science Foundation of China (Grant No.21776219), and the Postdoctoral Science Foundation of China (Grant No. 2018M631746).

References

1. J. T. Zhang and L. M. Dai, *Angew. Chem.-Int. Edit.*, 55 (2016) 13296.
2. Y. Zheng, Y. Jiao, L. H. Li, T. Xing, Y. Chen, M. Jaroniec and S. Z. Qiao, *ACS Nano*, 8 (2014) 5290.
3. G. L. Tian, M. Q. Zhao, D. S. Yu, X. Y. Kong, J. Q. Huang, Q. Zhang and F. Wei, *Small*, 10 (2014) 2251.
4. J. T. Zhang, Z. H. Zhao, Z. H. Xia and L. M. Dai, *Nat. Nanotechnol.*, 10 (2015) 444.
5. M. Mokhtar, M. Z. M. Talib, E. H. Majlan, S. M. Tasirin, W. Ramli, W. R. W. Daud and J. Sahari, *J. Ind. Eng. Chem.*, 32 (2015) 1.
6. L. M. Dai, Y. H. Xue, L. T. Qu, H. J. Choi and J. B. Baek, *Chem. Rev.*, 115 (2015) 4823.
7. A. Farnicola, S. Panero, B. Scrosati, M. Tamada and H. Ohno, *Chemphyschem*, 8 (2007) 1103.
8. R. Li, Z. D. Wei and X. L. Gou, *ACS Catal.*, 5 (2015) 4133.

9. Z. W. Chen, D. Higgins, A. P. Yu, L. Zhang and J. J. Zhang, *Energy Environ. Sci.*, 4 (2011) 3167.
10. R. Jasinski, *Nature*, 201 (1964) 1212.
11. S. Lee, Y. W. Lee, D. H. Kwak, J. Y. Lee, S. B. Han, J. I. Sohn and K. W. Park, *J. Ind. Eng. Chem.*, 43 (2016) 170.
12. F. Jaouen, E. Proietti, M. Lefevre, R. Chenitz, J. P. Dodelet, G. Wu, H. T. Chung, C. M. Johnston and P. Zelenay, *Energy Environ. Sci.*, 4 (2011) 114.
13. Z. L. Li, G. L. Li, L. H. Jiang, J. L. Li, G. Q. Sun, C. G. Xia and F. W. Li, *Angew. Chem.-Int. Edit.*, 54 (2015) 1494.
14. L. Lin, Q. Zhu and A. W. Xu, *J. Am. Chem. Soc.*, 136 (2014) 11027.
15. K. R. Seddon, A. Stark and M. J. Torres, *Pure Appl. Chem.*, 72 (2000) 2275.
16. R. D. Rogers and K. R. Seddon, *Science*, 302 (2003) 792.
17. J. Gao, N. Ma, J. F. Zha, T. Y. Li, W. Qin, T. T. Zhang and Z. Yin, *Ind. Eng. Chem. Res.*, 54 (2015) 7984.
18. D. Mecerreyes, *Prog. Polym. Sci.*, 36 (2011) 1629.
19. X. Q. Wang, C. D. Liang and S. Dai, *Langmuir*, 24 (2008) 7500.
20. T. P. Fellerger, A. Thomas, J. Y. Yuan and M. Antonietti, *Adv. Mater.*, 25 (2013) 5838.
21. J. S. Lee, X. Q. Wang, H. M. Luo and S. Dai, *Adv. Mater.*, 22 (2010) 1004.
22. J. Gao, N. Ma, Y. M. Zheng, J. F. Zhang, J. Z. Gui, C. K. Guo, H. Q. An, X. Y. Tan, Z. Yin and D. Ma, *ChemCatChem*, 9 (2017) 1601.
23. F. F. Dong, D. J. Chen, Y. B. Chen, Q. Zhao and Z. P. Shao, *J. Mater. Chem.*, 22 (2012) 15071.
24. V. B. Voitovich, V. V. Sverdel, R. F. Voitovich and E. I. Golovko, *Int. J. Refract. Met. Hard Mat.*, 14 (1996) 289.
25. L. Rabou and A. Roskam, *J. Power Sources*, 54 (1995) 316.
26. J. Gao, C. Shen, J. J. Tian, Z. Yin, H. B. Lu, J. Y. Feng, Y. Z. Huang and X. Y. Tan, *J. Appl. Electrochem.*, 47 (2017) 351.
27. W. Yang, T. P. Fellerger and M. Antonietti, *J. Am. Chem. Soc.*, 133 (2011) 206.
28. Y. C. Wang and X. Jiang, *ACS Appl. Mater. Interfaces*, 5 (2013) 11597.
29. C. W. B. Bezerra, L. Zhang, K. C. Lee, H. S. Liu, A. L. B. Marques, E. P. Marques, H. J. Wang and J. J. Zhang, *Electrochim. Acta*, 53 (2008) 4937.
30. D. Zhou, L. P. Yang, L. H. Yu, J. H. Kong, X. Y. Yao, W. S. Liu, Z. C. Xu and X. H. Lu, *Nanoscale*, 7 (2015) 1501.
31. X. J. Zhou, Z. Y. Bai, M. J. Wu, J. L. Qiao and Z. W. Chen, *J. Mater. Chem. A*, 3 (2015) 3343.
32. J. T. Zhang, L. T. Qu, G. Q. Shi, J. Y. Liu, J. F. Chen and L. M. Dai, *Angew. Chem.-Int. Edit.*, 55 (2016) 2230.
33. M. R. Wang, Z. Fang, K. Zhang, J. Fang, F. R. Qin, Z. A. Zhang, J. Li, Y. X. Liu and Y. Q. Lai, *Nanoscale*, 8 (2016) 11398.
34. G. Li, X. L. Wang, J. Fu, J. D. Li, M. G. Park, Y. N. Zhang, G. Lui and Z. W. Chen, *Angew. Chem.-Int. Edit.*, 55 (2016) 4977.
35. Q. Liu, Y. B. Wang, L. M. Dai and J. N. Yao, *Adv. Mater.*, 28 (2016) 3000.
36. Z. X. Wu, R. Liu, J. Wang, J. Zhu, W. P. Xiao, C. J. Xuan, W. Lei and D. L. Wang, *Nanoscale*, 8 (2016) 19086.
37. S. C. Cai, Z. H. Meng, H. L. Tang, Y. Wang and P. Tsiakaras, *Appl. Catal. B-Environ.*, 217 (2017) 477.
38. H. C. Tao, C. Yan, A. W. Robertson, Y. N. Gao, J. J. Ding, Y. Q. Zhang, T. Ma and Z. Y. Sun, *Chem. Commun.*, 53 (2017) 873.
39. Q. Xue, Z. X. Pei, Y. Huang, M. S. Zhu, Z. J. Tang, H. F. Li, Y. Huang, N. Li, H. Y. Zhang and C. Y. Zhi, *J. Mater. Chem. A*, 5 (2017) 20818.
40. J. Gao, C. C. He, J. G. Liu, P. J. Ren, H. B. Lu, J. Y. Feng, Z. G. Zou, Z. Yin, X. D. Wen and X. Y. Tan, *Catal. Sci. Technol.*, 8 (2018) 1142.
41. M. M. Hbssen, K. Artyushkova, P. Atanassov and A. Serov, *J. Power Sources*, 375 (2018) 214.

42. J. B. Zhu, M. L. Xiao, P. Song, J. Fu, Z. Jin, L. Ma, J. J. Ge, C. P. Liu, Z. W. Chen and W. Xing, *Nano Energy*, 49 (2018) 23.
43. Q. Xiang, S. Li, X. F. Zou, Y. J. Qiang, B. B. Hu, Y. Cen, C. L. Xu, L. J. Liu, Y. Zhou and C. G. Chen, *Appl. Surf. Sci.*, 462 (2018) 65.
44. J. Sun, S. E. Lowe, L. J. Zhang, Y. Z. Wang, K. L. Pang, Y. Wang, Y. L. Zhong, P. R. Liu, K. Zhao, Z. Y. Tang and H. J. Zhao, *Angew. Chem.-Int. Edit.*, 57 (2018) 16511.
45. C. Li, C. He, F. Sun, M. Wang, J. Wang and Y. Lin, *ACS Appl. Nano Mater.*, 1 (2018) 1801.
46. Y. S. Zhao, J. W. Wan, H. Y. Yao, L. J. Zhang, K. F. Lin, L. Wang, N. L. Yang, D. B. Liu, L. Song, J. Zhu, L. Gu, L. Liu, H. J. Zhao, Y. L. Li and D. Wang, *Nat. Chem.*, 10 (2018) 924.
47. Q. C. Wang, Y. J. Ji, Y. P. Lei, Y. B. Wang, Y. D. Wang, Y. Y. Li and S. Y. Wang, *ACS Energy Lett.*, 3 (2018) 1183.
48. Z. L. Li, Z. C. Zhuang, F. Lv, H. Zhu, L. Zhou, M. C. Luo, J. X. Zhu, Z. Q. Lang, S. H. Feng, W. Chen, L. Q. Mai and S. J. Guo, *Adv. Mater.*, 30 (2018) 1803220.
49. B. Li, S. P. Sasikala, D. H. Kim, J. Bak, I. D. Kim, E. Cho and S. O. Kim, *Nano Energy*, 56 (2019) 524.
50. H. Jiang, J. X. Gu, X. S. Zheng, M. Liu, X. Q. Qiu, L. B. Wang, W. Z. Li, Z. F. Chen, X. B. Ji and J. Li, *Energy Environ. Sci.*, 12 (2019) 322.
51. H. Han, Y. Noh, Y. Kim, W. S. Jung, S. Park and W. B. Kim, *Nanoscale*, 11 (2019) 2423.
52. L. J. Yang, G. C. Xu, J. J. Ban, L. Zhang, G. Xu, Y. Lv and D. Z. Jia, *J. Colloid Interface Sci.*, 535 (2019) 415.
53. Y. L. Lv, L. Yang and D. P. Cao, *ChemElectroChem*, 6 (2019) 741.
54. Y. H. Yu, Z. P. Zhang, L. M. Dai and F. Wang, *Chem.-Eur. J.*, 25 (2019) 5652.
55. H. W. Liang, X. D. Zhuang, S. Bruller, X. L. Feng and K. Mullen, *Nat. Commun.*, 5 (2014).
56. B. Y. Xia, Y. Yan, N. Li, H. B. Wu, X. W. Lou and X. Wang, *Nat. Energy*, 1 (2016).
57. S. Y. Wang, D. S. Yu and L. M. Dai, *J. Am. Chem. Soc.*, 133 (2011) 5182.
58. M. Perez-Alonso, K. Castro, I. Martinez-Arkarazo, M. Angulo, M. A. Olazabal and J. M. Madariaga, *Anal. Bioanal. Chem.*, 379 (2004) 42.
59. C. P. Leon, L. Kador, M. Zhang and A. H. E. Muller, *J. Raman Spectrosc.*, 35 (2004) 165.
60. M. A. Lopez-Manchado, J. Biagiotti, L. Valentini and J. M. Kenny, *J. Appl. Polym. Sci.*, 92 (2004) 3394.
61. S. Cobo, G. Molnar, J. A. Real and A. Bousseksou, *Angew. Chem.-Int. Edit.*, 45 (2006) 5786.
62. C. A. Tulk, J. A. Ripmeester and D. D. Klug, *Gas Hydrates: Challenges for the Future*, New York Acad Sciences, (2000) New York, USA.
63. P. Bharathidasan, D. W. Kim, S. Devaraj and S. R. Sivakkumar, *Electrochim. Acta*, 204 (2016) 146.
64. B. David, N. Pizurova, O. Schneeweiss, P. Bezdicka, J. Filip, R. Alexandrescu, I. Morjan, A. Crunteanu and I. Voicu, *Materials Structure & Micromechanics of Fracture IV*, Trans Tech Publications Ltd, (2005) Durnten-Zurich, Switzerland.
65. L. Xu, J. Shi, W. Q. Cao, M. Q. Wang, W. J. Hui and H. Dong, *J. Mater. Sci.*, 46 (2011) 3653.
66. M. Gruyters, *J. Magn. Magn. Mater.*, 248 (2002) 248.
67. A. S. W. Wong, G. W. Ho and D. Z. Chi, *J. Phys. D-Appl. Phys.*, 41 (2008) 042004.
68. K. Chokethawai, D. G. McCartney and P. H. Shipway, *J. Alloy. Compd.*, 480 (2009) 351.
69. J. C. C. Freitas, E. Nunes, E. C. Passamani, C. Larica, G. Kellermann and A. F. Craievich, *Acta Mater.*, 54 (2006) 5095.
70. R. Hirian, S. Mican, O. Isnard, L. Barbu-Tudoran and V. Pop, *J. Alloy. Compd.*, 697 (2017) 19.
71. A. Muthukrishnan, Y. Nabae, T. Okajima and T. Ohsaka, *ACS Catal.*, 5 (2015) 5194.
72. J. M. Ripalda, I. Montero and L. Galan, *Diam. Relat. Mat.*, 7 (1998) 402.
73. J. Zhang, D. P. He, H. Su, X. Chen, M. Pan and S. C. Mu, *J. Mater. Chem. A*, 2 (2014) 1242.
74. M. Q. Wang, W. H. Yang, H. H. Wang, C. Chen, Z. Y. Zhou and S. G. Sun, *ACS Catal.*, 4 (2014) 3928.
75. W. Ding, Z. D. Wei, S. G. Chen, X. Q. Qi, T. Yang, J. S. Hu, D. Wang, L. J. Wan, S. F. Alvi and L.

- Li, *Angew. Chem.-Int. Edit.*, 52 (2013) 11755.
76. K. A. Kurak and A. B. Anderson, *J. Phys. Chem. C*, 113 (2009) 6730.
77. Y. T. Liu, K. X. Li, Y. Liu, L. T. Pu, Z. H. Chen and S. G. Deng, *J. Mater. Chem. A*, 3 (2015) 21149.
78. F. P. Pan, Z. Y. Cao, Q. P. Zhao, H. Y. Liang and J. Y. Zhang, *J. Power Sources*, 272 (2014) 8.
79. J. L. Zhu, C. Y. He, Y. Y. Li, S. Kang and P. K. Shen, *J. Mater. Chem. A*, 1 (2013) 14700.
80. P. Wang, Z. K. Wang, L. X. Jia and Z. L. Xiao, *Phys. Chem. Chem. Phys.*, 11 (2009) 2730.
81. L. F. Lai, J. R. Potts, D. Zhan, L. Wang, C. K. Poh, C. H. Tang, H. Gong, Z. X. Shen, L. Y. Jianyi and R. S. Ruoff, *Energy Environ. Sci.*, 5 (2012) 7936.
82. J. Xu, H. T. Wu, X. Wang, B. Xue, Y. X. Li and Y. Cao, *Phys. Chem. Chem. Phys.*, 15 (2013) 4510.
83. J. N. Fiedor, W. D. Bostick, R. J. Jarabek and J. Farrell, *Environ. Sci. Technol.*, 32 (1998) 1466.
84. A. Ghahremaninezhad, D. G. Dixon and E. Asselin, *Electrochim. Acta*, 87 (2013) 97.
85. L. Z. Gu, L. H. Jiang, X. N. Li, J. T. Jin, J. H. Wang and G. Q. Sun, *Chin. J. Catal.*, 37 (2016) 539

© 2021 The Authors. Published by ESG (www.electrochemsci.org). This article is an open access article distributed under the terms and conditions of the Creative Commons Attribution license (<http://creativecommons.org/licenses/by/4.0/>).